# SINGLE-PHASE AND TWO-PHASE CFD SIMULATIONS OF THE COOLANT FLOW INSIDE A BRUCE/DARLINGTON CANDU FLOW CHANNEL

F. Abbasian, G. I. Hadaller, and R. A. Fortman

Stern Laboratories Inc.: 1590 Burlington Street East, Hamilton, Ontario, Canada L8H 3L3, fabbasian@sternlab.com

*Single-phase and two-phase flow computational fluid dynamics (CFD) simulations were performed for the coolant flow inside a CANDU thirty-seven element fuel string and the results are presented in this paper. The geometrical models represent original and modified 37-element fuel bundles inside un-crept and 5.1% crept pressure tubes. A Reynolds Averaged Navier Stokes (RANS) method with parallel processing was employed to limit the computational requirements to a reasonable level. The energy equations, decoupled from the momentum equations, were incorporated with a Conjugate Heat Transfer (CHT) model to investigate the element heat conduction effects. An inhomogeneous scheme in conjunction with a wall boiling and partitioning model was used for the two-phase flow analysis. Experiments were performed in a water loop with electrically-heated fuel bundles to simulate the fuel channel under a variety of operating conditions. Single-phase temperature and pressure and two-phase pressure data were used to evaluate the CFD model; good agreement was found. The CFD model was capable of predicting the pressure and temperature trends inside the flow channel as well as the bundle geometrical effects on the fuel thermalhydraulic performance.*

## I. INTRODUCTION

The flow of heavy water coolant passing through the subchannels of the fuel bundles inside CANDU fuel absorbs the heat generated by the fuel elements through the fission process. An understanding of the flow field inside the fuel channel is of importance. Highly uneven temperature distributions and excessive heat in the channels are not desirable and may lead to critical heat flux (CHF) phenomena. The coolant operating conditions of CANDU reactors are about 11 MPa pressure and temperatures as high as 310°C. As experiments at such operating conditions are both challenging and pricy, computer simulations are alternatively used to help understand the coolant flow behavior. The thermalhydraulic characteristics of the flow inside the channel depend highly on the particular arrangement of the fuel bundle elements, the heat flux profiles, the pressure tube deformations and other geometrical effects. An aging pressure tube has diametrical creep, resulting in different flow patterns towards the end of reactor life. Furthermore, the specific shape of the bundles and appendages play an important role in the formation of turbulent flow regimes. Hence, it is imperative that one include realistic geometrical features in the simulation process to obtain meaningful results.

Due to the high computational requirements for the modeling of the complicated geometries associated with the fuel bundle assemblies, most of the previous CFD works have been dedicated to subchannel models or simplified geometries (Refs 1, 2 and 3). A model was presented for a section of the CANDU 37-element bare-rod fuel bundle inside an un-crept channel. The turbulence intensity and kinetic energy patterns inside the subchannels and in the narrow-gap areas between the rods were provided (Ref. 4). It has been shown that particular fuel string assembly features, such as bundle-pressure tube eccentricity or pressure tube creep can alter the flow behavior inside the channel (Ref. 5). Also, the fuel bundle appendages and endplates induce cross flow regimes that promote mixing and may affect the heat transfer (Ref. 6). While some work has been done to study such effects in vertical assemblies (Refs. 7 and 8), more investigations are required for CANDU reactor applications. A model has been presented in Ref. 9 to investigate the bundle appendage effects in CANDU 6 and ACR1000 partial assemblies. The effects of the appendages on the flow are cumulative to the end of the channel. Under such circumstances, comprehensive 3-D simulations are required to study

the geometrical effects on the streamwise and spanwise flow development.

In the case of two-phase flow, the inherently complicated physics and the addition of mechanistic models make solutions even more challenging. Valuable work has been done in the area of two-phase flow modeling (Refs. 10 and 11). The first is an investigation of the effect that interfacial lift force modeling has on the predictions, and the second is a validation case for a wall partitioning model used for the flow inside a vertical heated tube. The modeling complications limit the work in this area to substantially simplified geometries and, as a result, fail to capture important geometrical effects. Little work has been done for full-scale or partial full-scale models. The work that has been done was generally in the area of vertical fuel assemblies (i.e Pressurized Water Reactors (PWR) and Boiling Water Reactors (BWR))

Full-scale CFD simulations for CANDU fuel channels have been presented previously by the authors (Refs 12 and 13). In this paper, the simulation results are compared against the Stern Labs experimental data. A description of the experimental set up and the CFD approach are given. ANSYS workbench software is used to model the coolant flow inside the fuel channel. The model features a pressure tube that contains twelve CANDU 37-element fuel bundles. The bundle geometries used in the experiments and in the CFD simulations are identical to the fuel bundles used in Bruce/Darlington reactors. Also, pressure tube creep and non-uniform axial and radial heat flux distributions are applied to the model and their effects are investigated. A steady-state Reynolds Averaged Navier-Stokes (RANS) method with a kinetic energy turbulence model was used for the single-phase model. For the two-phase flow simulation, an inhomogeneous scheme with a mechanistic wall boiling and partitioning model was employed.

## II. EXPERIMENTAL SET UP

The Bruce/Darlington CANDU 37-element fuel bundle, shown in Fig. 1, consists of a center element and three rings of fuel elements. There are 6, 12 and 18 elements in the inner, intermediate and outer rings surrounding the center element. The bundle also has endplates, spacers and bearing pads as shown in the figure. The diameter of each element is 13.08 mm and the overall length of the bundle is 495.3 mm. The diameter of the center element in a 37M bundle (modified 37-element) is 11.5 mm. A fuel channel consists of twelve bundles inside a pressure tube. The elements contain $UO_2$ pellets, which are subjected to the fission process to generate heat. The coolant flow passes through the areas in-between the elements, known as subchannels, and transfers the heat produced in the fission process to the steam generator.

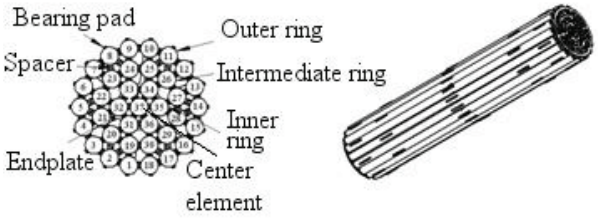


Fig. 1. CANDU 37-Element Fuel Bundle Original Design, Cross-Sectional and Isometric Views

The water loop constructed at Stern Labs can simulate the in-reactor operating conditions. Light water is used as the coolant and various operational conditions can be applied. A simplified schematic of the test loop is shown in Fig. 2. The test loop consists of a centrifugal pump, a test section, interconnecting piping, a steam/water separator, heat exchangers, flow control and metering stations, and a secondary cooling loop. The secondary loop contains two cooling towers. The loop was designed to operate at a maximum outlet pressure of 11 MPa and temperatures up to 310 °C.

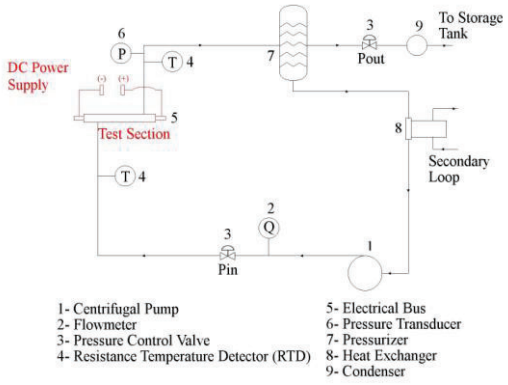


Fig. 2. Primary Test Loop Schematic

The test section, shown in Fig. 3, comprises a pressure housing, alumina ceramic liners which form the flow channel and provide electrical isolation of the fuel string, tee sections at each end for the inlet and outlet flow passages, and a fuel string which simulates twelve bundles. The pressure boundary consists of seven one-meter long spool pieces joined together and the two tee sections. The ceramic liners are machined to provide the desired creep profile. The diameter of the un-crept portion of the flow channel is 103.86 mm at 20 °C. As shown in Fig. 3, the flow channel diameter expands to a diametrical creep as high as 5.1% to simulate an aging reactor. The test section is instrumented with Differential Pressure Transducers (DP's), Absolute Pressure Transducers and Resistance Temperature Detectors (RTD's).

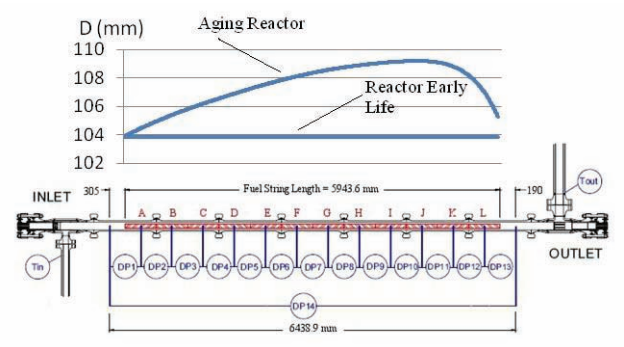


Fig. 3. Experimental Set Up: Test Section and the Pressure Tube Creep Profile

The fuel string simulation is an electrically heated 37-element, segmented design with a nominal 6 meter heated length and non-uniform, downstream skewed, axial heat flux distribution and radial flux distribution as shown in Figure 4. The fuel string consists of twelve fully aligned bundles, designated "A" to "L", with external geometry the same as real fuel bundles representative of the Bruce/Darlington design. The axial and radial heat flux distributions are accomplished by varying the wall thickness of the heater tubes (while maintaining a constant outside diameter). The bundles have simulated end plates and hollow spacers and bearing pads. The heat flux profile used in the present study is shown in Fig. 4. The highest and lowest power ratios belong to the outer ring and center element, respectively, and the peak power in the axial direction occurs at bundle H. The element wall thickness was calculated based on the total power and the given axial and radial profiles.

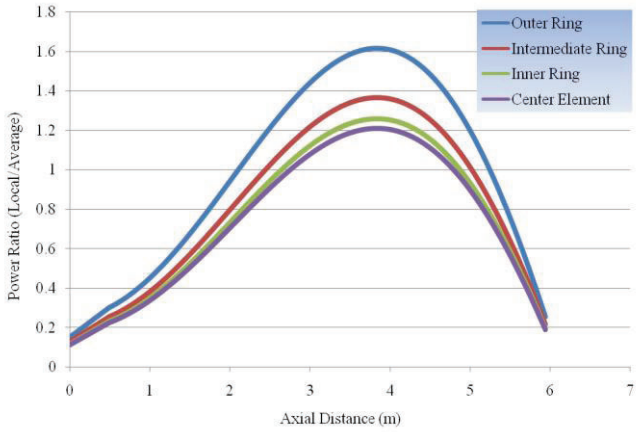


Fig. 4. Axial and Radial Heat Flux Distribution

The fuel string is instrumented with internal thermocouples for CHF detection in most of the heater elements in the downstream half of the fuel string. The thermocouples are mounted in moveable ceramic carriers to measure temperatures at the inside wall of heater elements in bundles H through L. Fig. 5 schematically shows the thermocouple instrumentation reference locations in a heater element. A thermocouple drive mechanism is used to remotely move the carriers axially and rotate them to cover most of the instrumented surface area (89%). Pressure taps are located 25 mm upstream of each bundle midplane for differential and absolute pressure measurements.

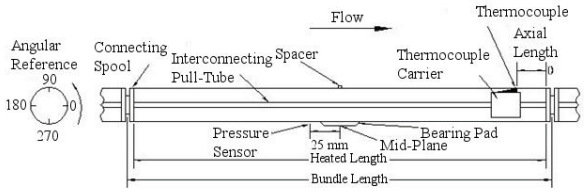


Fig. 5. Instrumentation: Thermocouple Drive System and Pressure Sensor Location

## III. COMPUTATIONAL MODEL

The computational domain is shown in Fig. 6. For single-phase simulations, all twelve bundles are included in the geometrical model, while for two-phase simulations, bundles E to H are included. The 3-D steady-state RANS equations with the kinetic energy turbulence model are solved in conjunction with the continuity and energy equations in a segregated pressure-based solver. The unsteady governing equations for each phase may be written as follows:

Continuity equation:

$$\frac{\partial}{\partial t}(\alpha_l \rho_l) + \nabla \cdot (\alpha_l \rho_l \vec{u}_l) = \sum_{g=1}^{n} \dot{m}_{\mathrm{lg}} A_{\mathrm{lg}} \qquad (1)$$

Momentum equation:

$$\frac{\partial}{\partial t}(\alpha_l \rho_l \vec{u}_l) + \nabla \cdot (\alpha_l \rho_l \vec{u}_l \vec{u}_l) = -\alpha_l \nabla p + \nabla \cdot \vec{\tau}_l + \sum_{g=1}^{n} (\dot{m}_{\mathrm{lg}} A_{\mathrm{lg}} \vec{u}_g - \dot{m}_{gl} A_{gl} \vec{u}_l) + M + \alpha_l \rho_l g \qquad (2)$$

Energy equation:

$$\frac{\partial}{\partial t}(\alpha_l \rho_l e_l) + \nabla \cdot (\alpha_l \rho_l \vec{u}_l e_l) = \nabla \cdot (\alpha_l K_l \nabla T_l) + \nabla \vec{u}_l . \vec{\tau}_l + \sum_{g=1}^{n} (\dot{m}_{\mathrm{lg}} A_{\mathrm{lg}} e_g - \dot{m}_{gl} A_{gl} e_l) + Q \qquad (3)$$

The two-phase flow model includes Eulerian-Eulerian methodology with water as the continuous and vapor as the dispersed (gaseous) phase. The equations are generalized based on the assumption of the continuous phase being incompressible. The inhomogeneous equations are solved in conjunction with a wall boiling model that employs a wall partitioning method (Ref. 14) to define heat transfer patterns based on the local subcooling temperatures. As a result, the wall heat transfer patterns vary along the channel, which is a more realistic presentation of the two-phase flow development in a reactor fuel channel. The term "M" in the momentum equations (Eq. (2)) consists of empirical equations for interfacial drag and lift forces (Ref. 15). The Ishii-Zuber drag model (Ref. 16), suitable for bubbles and droplets, was used to model the interfacial drag force.

For the two-phase flow simulations the computational domain was limited to bundles E to H to reduce the high computational demands. The inlet conditions were imported from single-phase results.

An upwind differencing scheme with second-order accuracy was used for the momentum equations, and under-relaxation factors were applied whenever convergence related issues arose. An unstructured mesh was used for the irregular geometries associated with the appendages, and a quadrilateral mesh was used for the tubular components. The mesh specifications for the single-phase models are shown in TABLE I. The computations were performed using the parallel processing of 16 processors in an Intel ® Xeon ® CPU 2.67 GHz system and 64 GB of RAM. Convergence of the momentum equations took 690 iterations for the single-phase models and 910 iterations for the two-phase models. The single-phase and two-phase flow simulations were performed using ANSYS Fluent and CFX, V14.5, respectively.

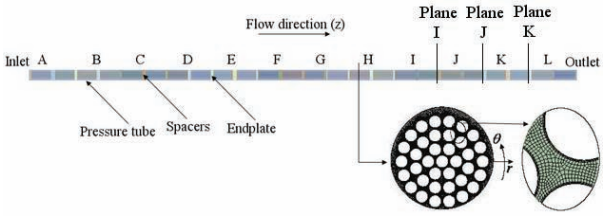


Fig. 6. Computational Model: Bundles A to L inside the Pressure Tube, Cross Sectional Mesh and the Coordinate System

TABLE I. Mesh Specifications

| | |
|---|---|
| Grid size | $52\times10^{6}$ |
| $y^{+}$ | 5 |
| $\Delta r$ ($\times10^{-3}$ m) | 0.2-0.7 |
| $r^{+}$ | 10-35 |
| $r\Delta\theta$ ($\times10^{-3}$ m) | 0.4-1.6 |
| $(r\theta)^{+}$ | 20-80 |
| $\Delta z$ ($\times10^{-3}$ m) | 0.5-5 |
| $z^{+}$ | 25-250 |

## IV. BOUNDARY CONDITIONS

A no-slip wall boundary condition is applied to all solid surfaces. The fluid inlet flow and temperature, and outlet pressure from the experimental data are used as the inlet velocity and outlet pressure boundary conditions. The heat flux profiles shown in Fig. 4 are applied to the element surfaces. The single-phase and two-phase boundary conditions are shown in TABLE II. The two-phase flow conditions from an initial dryout test were used.

TABLE II. Boundary Conditions

| Boundary Conditions | Mass flow Rate (Kg/s) | Total Power (MW) | Inlet Temperature (°C) | Outlet Pressure (MPa) |
|---|---|---|---|---|
| Single-phase | 13.5 | 2.00 | 180 | 9 |
| Two-phase | 19.0 | 7.13 | 265 | 10 |

## V. RESULTS AND DISCUSSION

The pressure and temperature patterns obtained from running the simulations are compared to experimental data. The simulation models were run for crept and un-crept channels with original and modified 37-element fuel bundles. The pressure measurements are taken at fixed locations 25 mm upstream of each bundle midplane, and the temperature measurements are taken at various azimuthal locations on each heater element and about 17 mm upstream of the downstream end of the heated length (endplates) (see Fig. 5). The ceramic carriers containing the thermocouples are rotated using stepping motors at a speed of about 6 °/s. The time increment of the data acquisition system is 0.1 s (10 Hz) which gives a resolution in the azimuthal direction of about 0.6 °. The carriers in bundles J and K contain two thermocouples 180 ° apart.

### V.a. Single-Phase Velocity and Temperature Results

The velocity contours, shown in Fig. 7, as expected show that high flow velocities are seen at the subchannel centers (inflow) and the velocities gradually decrease towards the rod surfaces to approximate the no-slip condition. The maximum velocity values at the subchannel centers vary from 0.79 to 1.64 times the average velocity. The eccentricity of the bundle in the crept pressure tube produces a flow bypass that results in higher velocities at the top and lowest at the center.

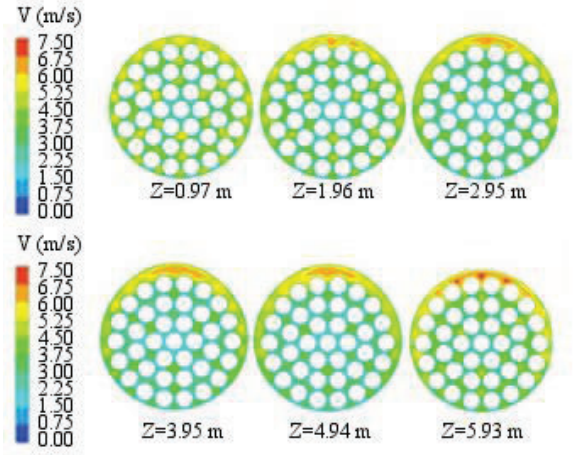


Fig. 7. Single-Phase Flow Velocity Contours for the Crept Channel

The temperature contours are obtained by interpolation of the surface temperatures for each cross section plane and are shown in Fig. 8. The contour plane of each bundle is located at 17 mm upstream of the end of the heated length which is the location of the thermocouples in the experiments (bundles I, J and K shown in Fig. 6). The temperature contours indicate that the high and low temperatures occur at the center and top of the channel, respectively. Due to the larger flow areas in the top of the channel, the subchannels surrounding the center element experience lower flows, hence higher temperatures. The temperature maxima and minima and their locations are predicted well by the model. The flow asymmetry evident in the experimental data is captured by the CFD model. The source of the flow asymmetry is believed to be the turbulence induced by the bundle appendages. The turbulence in the subchannels has both coherent and non-coherent structures and can exhibit highly anisotropic behavior (Ref. 17). The secondary flow regimes are generated by the appendages and produce vortices inside the subchannels that grow and change

direction with time. An unsteady simulation, preferably with a non-averaged (direct or semi-direct) simulation such as large eddy simulation (LES) or Reynolds stress model (Ref. 18), would more accurately model turbulence structures and their evolution with time. Such models could further improve the prediction of turbulence mixing compared to the current RANS method.

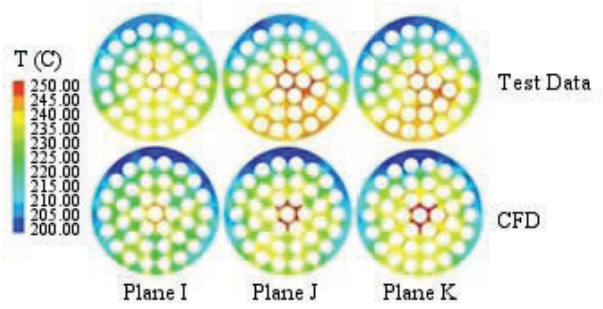


Fig. 8. Single-Phase Temperature Contours for the Crept Channel

As shown in the velocity and temperature contours, the flow by-pass caused by the pressure tube creep results in an uneven cross-sectional temperature distribution. In order to improve the performance of the fuel, the diameter of the center element of the Bruce/Darlington 37-element fuel bundle was reduced from 13.08 mm to 11.5 mm, thereby allowing more flow through the center of the bundle. The temperature contours for the original and modified 37-element models are shown in Fig. 9. The effect of the geometric changes on the flow field, captured by the CFD model, resulted in lower temperatures at the center of the bundle and a relatively more even temperature distribution compared to the original fuel design. This modification has provided improved CHF performance.

The computational domain consists of fluid medium and solid boundaries (i.e. the fuel bundles and the pressure tube). The solid parts can be treated as a surface boundary condition with a solver-calculated surface heat transfer coefficient, however the effect of conduction heat transfer inside the solid parts is missed. In order to investigate such effects, a Conjugate Heat Transfer (CHT) model was used and the element wall thicknesses and material properties were defined for the solid boundaries. The element surface temperatures for the hottest and coldest elements are shown in Fig. 10. The circumferential temperature variation is a function of element position and proximity to the adjacent elements. As shown in Fig. 10, the CHT model improves the predictions by modeling the diffusion inside the solid boundaries.

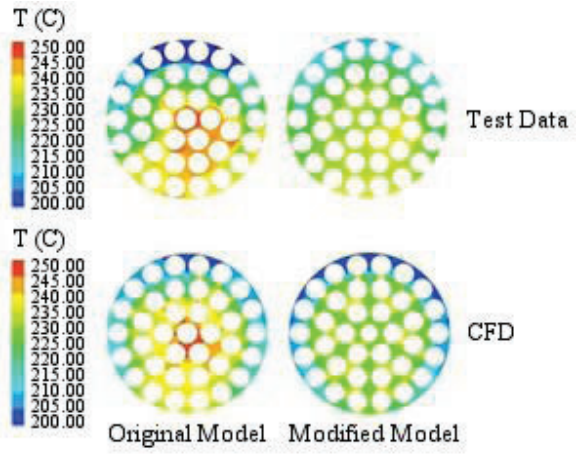


Fig. 9. Single-Phase Temperature Contours at the Flow Channel Outlet for the Original and Modified (Smaller Center Element Diameter) 37-Element Fuel Bundles

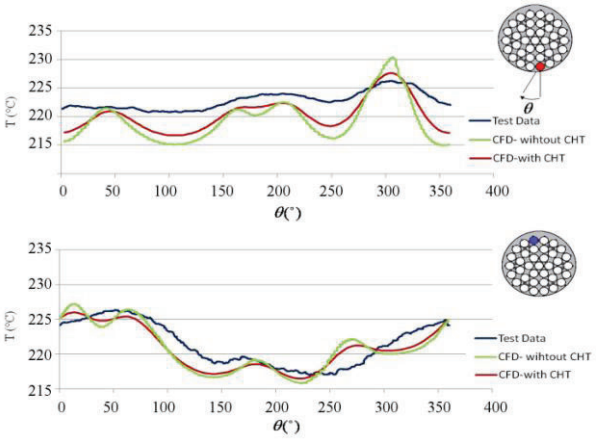


Fig. 10. Circumferential Temperature Variations on the Hot and Cold Elements for the Modified 37-Element Bundle; CHT Effects

### V.b. Single-Phase Pressure Results

The total channel pressure drop variation with flow rate for the model was compared to the experimental data in Fig. 11. The channel pressure drop from the experiments was obtained by summation of the DP2 to DP11 differential pressures (see Fig. 3). The CFD results are in good agreement with the experimental data for the flow range 7-20 kg/s.

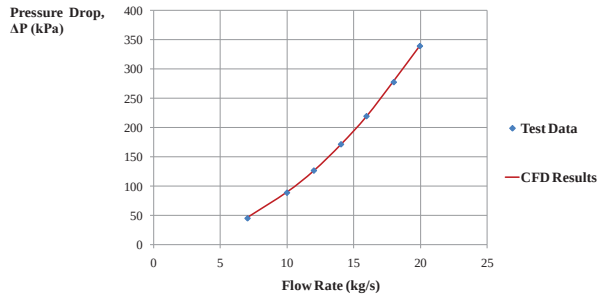


Fig. 11. Single-Phase Channel Pressure Drops for the Modified 37-Element Un-crept Channel

### V.c. Two-Phase Flow Void Distributions

The local vapor void fractions and their variation along the fuel channel for the two-phase flow condition given in TABLE II are shown in Fig. 12. Similar to the single-phase analysis, the relatively low flow rates at the channel center account for highest void fractions occurring in that area. It is noteworthy that while flow mixing and heat transfer are enhanced downstream of the appendages, void fractions are higher locally on the upstream side as a result of wake turbulence and stagnation.

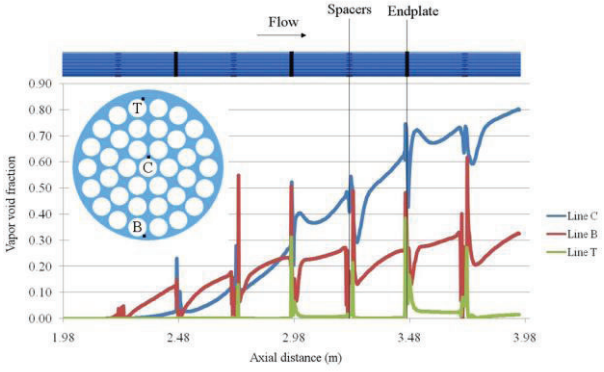


Fig. 12. Local Void Fraction Variations in Axial Direction for the Original 37-Element Model (under Initial Dry-Out Conditions)

### V.d. Two-Phase Pressure Drop

As there was no means available for the validation of void predictions against the experimental data, a two-phase flow pressure analysis was used for validation. The pressure drop profile along the pressure tube in a two-phase flow state is significantly different from that of the single-phase state. For a crept channel, the local single-phase bundle pressure drop decreases in the axial direction as a result of the channel creep with larger flow areas. For the two-phase flow state, the dispersed phase is a source of interfacial drag force that increases the pressure drop. At some point along the flow channel, the two-phase flow effect becomes dominant and outweighs the effect of the channel creep (larger flow area). This turning point represents the location of Onset of Significant Void (OSV). A series of OSV tests were performed in the experiments at Stern Labs at the conditions given in TABLE III, where the flow rate was kept constant and the power was gradually raised until the bundle pressure drop increase was observed.

TABLE III. Onset of Significant Void (OSV) Test Conditions

| Power (MW) | Flow (Kg/s) | Inlet Temperature (ºC) | Outlet Pressure (MPa) | Exit Quality (%) |
|---|---|---|---|---|
| 3.401 | 17.02 | 255.3 | 9.011 | -3.8 |
| 3.801 | 17.01 | 254.9 | 9.006 | -2.2 |
| 4.200 | 17.02 | 255.1 | 9.026 | -0.5 |
| 4.599 | 17.02 | 255.0 | 9.029 | 1.1 |
| 5.000 | 17.03 | 254.8 | 9.015 | 2.8 |
| 5.400 | 17.02 | 255.0 | 8.989 | 4.6 |

The pressure drop results obtained from the two-phase model are compared with the OSV data from the experiments in

Fig. 13. The two-phase flow effects on pressure drop is captured by the CFD model for the full range of exit qualities. The pressure drop ratio at the highest exit quality of 4.6% is 1.14 for the test data and 1.10 for the CFD model. The two-phase flow effect on DP2 is more pronounced for the CFD results compared to the experimental data. This discrepancy may indicate inaccurate wall heat transfer and bubble departure modeling that gives rather unrealistic void development

along the channel. For a more accurate evaluation of the two-phase flow solver, void distribution experimental data are required to independently investigate this phenomenon.

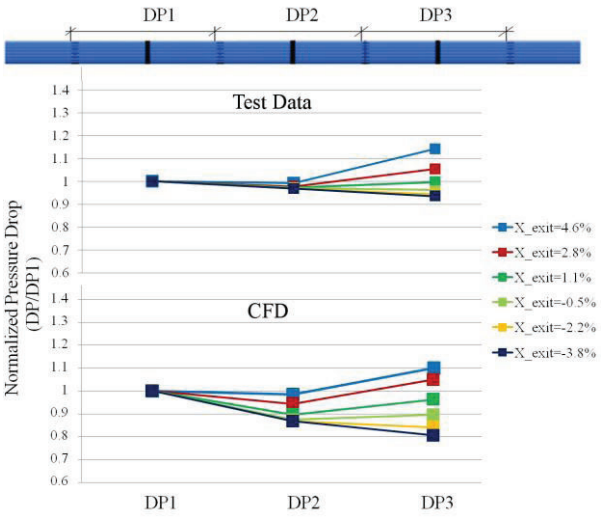


Fig. 13. Two-Pressure Drop vs. Exit Quality (X_exit) for the Original 37-Element Model in a Crept Channel

## VI. CONCLUSIONS

Single-phase and two-phase flow RANS CFD simulations were performed for the Bruce/Darlington fuel channels and the results were presented in this paper. The simulations featured full scale geometrical modeling of the fuel channel containing twelve 37-element fuel bundles. The pressure tube creep and bundle design modification were included in the analysis. Experimental facilities existing at Stern Labs use electrically heated fuel string simulations. In-reactor conditions were applied and various thermalhydraulic tests, including Heat Balance, CHF, Dryout and Post Dryout tests were performed. The CFD results were compared against the Stern Labs experimental data.

The single-phase results are in good agreement overall with the test data. The cross sectional temperature distributions and the location of hot spots were predicted well by the CFD models. The models were sensitive enough to capture geometrical effects, such as the pressure tube creep or bundle design changes, on the flow field. The Conjugate Heat Transfer (CHT) approach improved the solution by modeling heat conduction inside the solid boundaries. It is believed that more advanced turbulence models, such as Large Eddy Simulation (LES), albeit at a higher computational cost, would provide more accuracy with regard to the simulation of the flow mixing and velocity-temperature fields.

The two-phase flow solver employed an inhomogeneous scheme with a wall boiling model that accounts for wall heat transfer variations with local subcooling temperatures. The pressure drop results for two-phase flow conditions were compared against the Onset of Significant Void (OSV) test data. The effect of two-phase flow on the pressure drop at known exit qualities was captured by the CFD model similar to the patterns observed in the experiments. Independent experimental data are required to evaluate the void distribution predictions for the two-phase CFD model.

The developed CFD methodology is useful for understanding the coolant flow behavior and predicting geometrical effects on thermalhydraulic performance of nuclear fuel in reactors.


## ACKNOWLEDGEMENT

The authors would like to thank the team of technologists at Stern Labs for their assistance in the experimental set up.

## NOMENCLATURE

| | |
|---|---|
| $A_{lg}$ | specific interfacial area between the liquid and gas phases (1/m) |
| $e$ | internal energy (J/kg) |
| $g$ | gravitational acceleration (9.8 m/s$^2$) |
| $K$ | conductivity (Wm$^{-1}$K$^{-1}$) |
| $M$ | sum of the interfacial forces (N/m$^3$) |
| $\dot{m}_{\mathrm{lg}}$ | mass flow rate per unit interfacial area (kgm$^{-2}$s$^{-1}$) |
| $P$ | pressure (Pa) |
| $Q$ | interfacial heat transfer (W/m$^3$) |
| $T$ | temperature (K) |
| $t$ | solution time (s) |
| $\vec{u}$ | velocity field (m/s) |
| $y^+$ | Dimensionless wall distance |

*Greek letters*

| | |
|---|---|
| $\alpha$ | volume fraction |
| $\mu_l$ | liquid viscosity (kgm$^{-1}$s$^{-1}$) |
| $\rho$ | density (kgm$^{-3}$) |

*Subscripts*

| | |
|---|---|
| $g$ | gas |
| $l$ | liquid |

## REFERENCES


1. K. B. Lee and H. C. Jang, H.C., "A Numerical Prediction on the Turbulent Flow in Closely Spaced Bare Rod Arrays by a Nonlinear *k*-ε Model" *Journal of Nuclear Engineering and Design*, **172**, 351–357 (1997).

2. W. K. In, C. H. Shin, D. S. Oh and T. H. Chun, "CFD Simulation of the Turbulent Flow and Heat Transfer in a Bare Rod Bundle" *Proceedings of ICAPP'04, Pittsburgh, PA, USA*, June 13-17, pp. 1544-1551, Paper 4179 (2004).

3. E. Baglietto and H. Ninokata, "A Turbulence Model Study for Simulating Flow Inside Tight Lattice Rod Bundles" *Journal of Nuclear Engineering and Design*, **235**, 773-784 (2005).

4. D. Chang and S. Tavoularis, "Numerical Simulation of Turbulent Flow in a 37-rod Bundle" *Journal of Nuclear Engineering and Design*, **237**, 575-590 (2007).

5. F. Abbasian, S. D. Yu and J. Cao, "Parallel CFD Simulations of Turbulent Flows inside a CANDU Fuel Bundle" *10th CNS International Conference on CANDU Fuel, Toronto,* October 5-8 (2008).

6. F. Abbasian, S. D. Yu and J. Cao, "Experimental and Numerical Investigations of Three-Dimensional Turbulent Flow of Water Surrounding a CANDU Simulation Fuel Bundle Structure inside a Channel" *Journal of Nuclear Engineering and Design*, **239**, 2224-2235 (2009).

7. K. Ikeda, Y. Makino and M. Hoshi, M., "Single-Phase CFD Applicability for Estimating Fluid Hot-Spot Locations in a 5×5 Fuel Rod Bundle" *Journal of Nuclear Engineering and Design*, **236**, 1149-1154 (2006)

8. B. S. Shin, B and S. H. Chang, "CHF Experiment and CFD Analysis in a 2×3 Rod Bundle with Mixing Vane" *Journal of Nuclear Engineering and Design*, **239**, 899–912 (2009).

9. A. Catana, et al., "Computational Fluid Dynamics Approach for CANDU6 and ACR1000 Fuel Channel Coolant Flow" *U.P.B. Sci. Bull.,* Series D, Vol. 72, Iss. 1 (2010).

10. A. Tentner, S. Lo, A. Ioilev, V. Melnikov, M. Samigulin, V. Ustinenko and V. Kozlov, "Advances in Computational Fluid Dynamics Modeling of Two-Phase Flow in a Boiling Water Reactor Fuel Assembly" *Proceedings of ICONE14 International Conference on Nuclear Engineering*, July 17-20, Miami, Florida, USA (1996).

11. E. Krepper, B. Koncar and Y. Egorov, "CFD Modelling of Subcooled Boiling—Concept, Validation and Application to Fuel Assembly Design" *Journal of Nuclear Engineering and Design*, **237**, 716–731 (2007).

12. F. Abbasian, G. I. Hadaller and R. A. Fortman, "CFD Simulations of the Single-Phase and Two-Phase Coolant Flow of Water inside the Original and Modified CANDU 37-Element Bundles" *11th International Conference on CANDU Fuel Sheraton Fallsview Hotel and Conference Centre Niagara Falls, Ontario, Canada,* October 17-20 (2010).

13. F. Abbasian, G. I. Hadaller and R. A. Fortman, "Advanced CFD Simulations of Turbulent Flows around Appendages in CANDU Fuel Bundles" *12th International Conference on CANDU Fuel Holiday Inn Waterfront Hotel Kingston, Ontario, Canada*, September 15-18 (2013).

14. N. Kurl and M. Z. Podowski, "On the Modeling of Multidimensional Effects in Boiling Channels" *ANS Proc. 27th National Heat Transfer Conference, Minneapolis, MN,* July 28-31 (1991).

15. ANSYS Workbench 14.5 Documentation

16. M. Ishii, and N. Zuber, "Drag Coefficient and Relative Velocity in Bubbly, Droplet or Particulate Flows", AIChE J., **25**, 843-855, (1979).

17. F. Abbasian, S. D. Yu and J. Cao, "Large Eddy Simulation of Turbulent Axial Flow along an Array of Rods" *ASME J. Fluids Eng.,* **132**(2), 021105 (11 pages) (2010).

18. D. Chang and S. Tavoularis, "Numerical Simulations of Developing Flow and Vortex Street in a Rectangular Channel with a Cylindrical Core" *Journal of Nuclear Engineering and Design*, **243**, 176–199 (2012).